INSTITUTE OF PHYSICS PUBLISHING PHYSICS IN MEDICINE AND BIOLOGY

Phys. Med. Biol. **47** (2002) 1167–1184 PII: S0031-9155(02)27436-9

The effect of volume currents due to myocardial anisotropy on body surface potentials

Ceon Ramon[1], Paul Schimpf[2], Yanqun Wang[3], Jens Haueisen[4] and Akira Ishimaru[1]

[1] Department of Electrical Engineering, University of Washington, Seattle, WA, USA
[2] Department of Electrical Engineering and Computer Science, Washington State University, Spokane, WA, USA
[3] Rosetta Inpharmatics, Inc., Kirkland, WA 98034, USA
[4] Biomagnetics Center, F. S. University, Jena, Germany

E-mail: ceon@u.washington.edu

Received 1 August 2001, in final form 18 January 2002
Published 20 March 2002
Online at stacks.iop.org/PMB/47/1167

Abstract

Changes in anterior and posterior body surface potential maps (BSPMs) due to myocardial anisotropy were examined using a highly heterogeneous finite element model of an adult male subject constructed from segmented magnetic resonance images. A total of 23 different tissue types were identified in the whole torso. The myocardial fibre orientations in the human heart wall were mapped from the fibre orientations of a canine heart which are available in the literature using deformable mapping techniques. The current and potential distributions in the whole torso were computed using dipolar sources in the septum, apical area, left ventricular wall or right ventricular wall. For each dipole x, y, z orientations were studied. An adaptive finite element solver was used to compute currents and potential distributions in the whole torso with an element size of $0.78 \times 0.78 \times 3$ mm in the myocardium and larger elements in other parts of the torso. For each dipole position two cases were studied. In one case the myocardium was isotropic and in the other it was anisotropic. It was found that BSPMs showed a very notable difference between the isotropic and the anisotropic myocardium for all dipole positions with the largest difference for the apical dipoles. The correlation coefficients for the BSPMs between the isotropic and anisotropic cases ranged from 0.83 for an apical dipole to 0.99 for an RV wall dipole. These results suggest that myocardial fibre anisotropy plays an important role in determining the body surface potentials.

(Some figures in this article are in colour only in the electronic version)

1. Introduction

Body surface potential maps (BSPMs) are being explored as a tool for detection and diagnoses of electrocardiac disorders (Stroink *et al* 1999, Aiba *et al* 2000, Pinter *et al* 2000). These maps are also being used to solve the inverse problems for localizing the sites of abnormal electrical activity in the heart (Hren *et al* 1996, 1998b). It has also been shown that the epicardial potentials during paced activation are also affected by myocardial fibre anisotropy (Hren *et al* 1998a). The electrical activity of the heart is known to be strongly influenced by the myocardial fibre anisotropy (Plonsey 1974, Streeter 1979, Colli-Franzone *et al* 1998, Lorange and Gularjani 1993). Thus, it becomes important to examine in detail how the myocardial fibre anisotropy influences the BSPMs.

The secondary volume currents flowing in the heart wall are affected by the myocardial fibre anisotropy (Ramon *et al* 2000). The subsequent flow of the volume currents in the torso would eventually affect the BSPMs. Recently, it has been shown that torso inhomogeneities have some minor effects on BSPMs relative to a homogeneous torso (Ramanathan and Rudy 2001). The size of the torso is large compared to that of the heart and it tends to smooth out the volume currents emanating from the myocardium. However, even then the volume currents spreading out of an anisotropic myocardium could still change the BSPMs. Also, the apparent degree of smoothing effects of the torso could be related to the complexity of the computer models of the heart and torso. A simpler model of the torso with only a few (2–4) compartments could tend to smooth out the anisotropy-dependent current flow patterns more compared to a highly heterogeneous torso model.

To accurately model the volume currents in the torso, one needs to use a high-resolution heterogeneous model of the torso in which all the major tissue types have been identified. Such highly accurate models have been used earlier by us for simulating the magnetocardiograms in normal and infarcted hearts (Ramon *et al* 1998, Czapski *et al* 1998), to study the effects of tissue conductivities on the torso magnetic fields (Czapski *et al* 1996a) and how volume currents from different tissue types contribute to the total torso magnetic fields (Czapski *et al* 1996b). Similar high-resolution models should also be used for examining the effect of the myocardial fibre anisotropy on the BSPMs. In this paper, we examined the changes in the BSPMs due to myocardial fibre anisotropy by using a high-resolution ($0.78 \times 0.78 \times 3$ mm) highly heterogeneous (23 tissue types) finite element model of the heart and torso.

In a recent study we have shown that myocardial fibre anisotropy affects the current flow patterns and magnetic fields for a dipolar source in the septum of the heart wall (Ramon *et al* 2000). In that study we examined also the influence of myocardial anisotropic conductivity on the BSPMs. Our previously reported results were only for a z-oriented single dipole in the septum of the heart. The results reported here are an extension of our work for x-, y- and z-oriented dipolar sources in different areas of the heart walls, i.e., in the septum, left ventricular (LV) wall, right ventricular (RV) wall and apical area of the heart. It was found that for all dipolar positions, the anterior and posterior BSPMs were influenced by myocardial fibre anisotropy.

2. Methods

Our procedures for building the heart–torso model and computing the current distribution and potentials are described elsewhere (Ramon *et al* 1998, 2000, Czapski *et al* 1996a, 1996b, 1998). A brief review of our methods is given here. We used magnetic resonance imaging (MRI) data of an adult male subject without any known heart problems for constructing a high-resolution model of the heart and torso. MRI data were collected at the University of

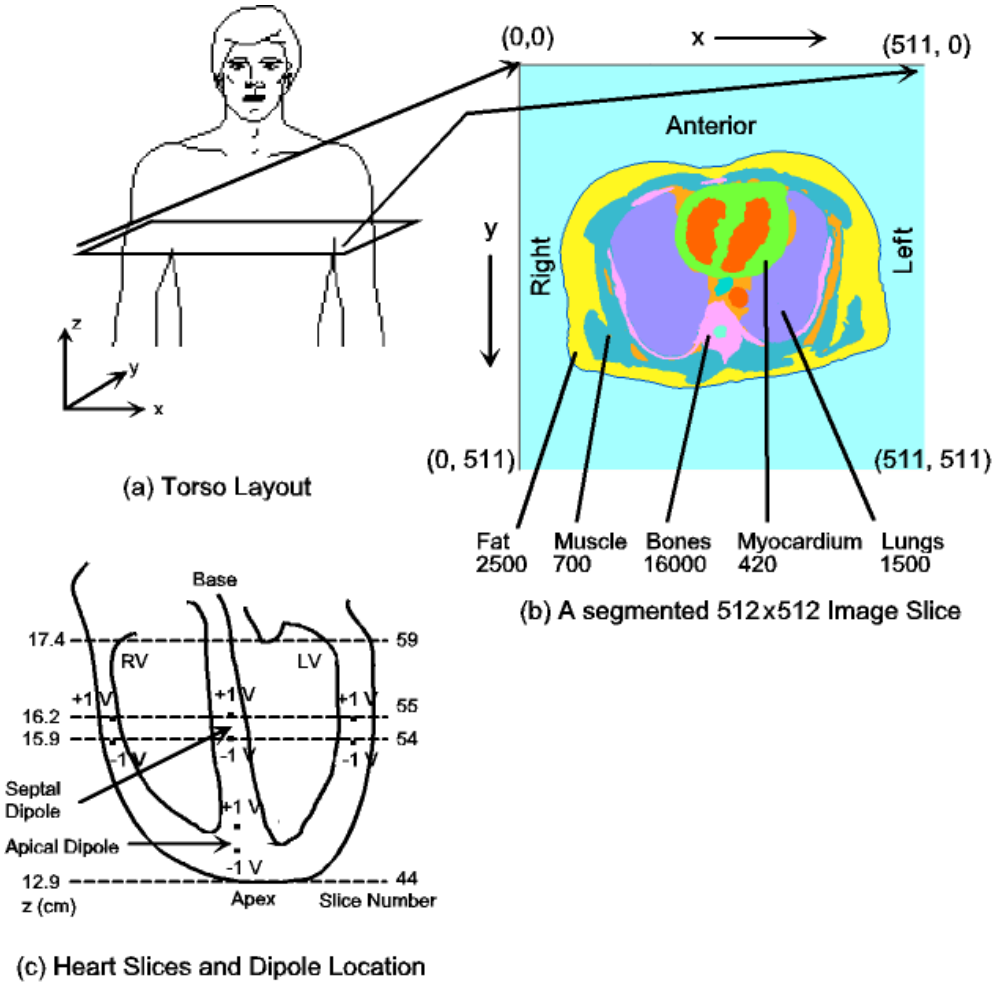

Figure 1. (a) A layout of the torso shape and the orientation of the coordinates, (b) details of the image slices in the heart area and (c) the location of the dipolar sources in the septum, apex, LV and RV walls.

Washington Medical Center, Seattle, WA with a GE Signa 1.5 T MRI machine. Each proton density MRI slice was collected with cardiac gating to reduce the motion artefacts. The MRI data were collected when the heart was in the diastolic state. The entire scan consisted of 52 transaxial slices with a 6 mm vertical separation. Each slice has a 256 × 256 pixel resolution with a field of view of 40 × 40 cm. An additional 51 images were generated between the original slices by linear interpolation, resulting in a total of 103 images with a 3 mm vertical separation. Similarly, each slice was interpolated to 512 × 512 pixels. This provides a pixel resolution of 0.78 × 0.78 mm for a given field of view of 40 × 40 cm. The above enhancements were done to provide a finer grid spacing in the horizontal and vertical directions for insertion of the electrical sources in the finite element model of the heart. A semi-automatic tissue classification software developed by us was used to classify the MR images (Shrinidhi *et al* 1996). A total of 23 different tissue types were identified in the whole torso.

A layout of the torso surface and coordinate orientation is shown in figure 1(a). One of the segmented torso slices with different tissue types is shown in figure 1(b). The tissue types

and the respective tissue resistivities (Ω cm) are also included. A schematic representation of the heart wall, image slices in the heart and location of dipoles is shown in figure 1(c). The increasing x direction is from the right to the left of the subject, the increasing y direction is from the front (anterior) to the back (posterior) of the subject and the increasing z direction is from the abdomen (inferior) to the shoulders (superior). This gives us an anticlockwise ($x \times y = z$) coordinate system for computations. The first image slice of the torso, i.e. slice number 1, is located at $z = 0$ cm at the upper abdomen area. The last of the image slices, i.e. slice number 103, is located at $z = 102 \times 0.3 = 30.6$ cm at the upper chest area. As shown in figure 1(b), the bottom of the heart, i.e. the apex, is located in slice number 44 at $z = 12.9$ cm. The top of the ventricles is in slice number 59, and the top of the heart is located in slice number 67 at $z = 19.8$ cm, which is not shown in the figure.

A complete data set of ventricular fibre orientation for the human heart is unavailable in the literature. However, it has been found that the heart fibre structure is very similar across various mammalian species (Streeter 1979). A complete data set of the fibre orientation of a canine heart has been mapped at the University of Auckland in New Zealand (Nielsen *et al* 1991), and it is available at their website on the Internet. This data set is also being used by other research groups for incorporating the fibre anisotropy into computer models of the heart (Eason *et al* 1998, Wang *et al* 2001). We mapped the fibre orientations from the canine heart to our adult male subject's human heart using deformable mapping techniques (Foley 1995, Wang *et al* 2001).

A finite element mesh with rectangular parallelopiped (brick-shaped) elements was generated in the whole torso. We used the smallest elements of size $0.78 \times 0.78 \times 3$ mm^3 in the heart wall and larger size elements in other parts of the torso. An adaptive finite element solver developed by us was used for all the computational work (Schimpf *et al* 1996, 1998). A dipole of +1 and −1 V was placed between slices 55 and 54 in the middle of the septum. Similar dipole locations were used in the RV and LV walls, and also in the mid-apical area of the heart. Only one dipole was used in each simulation. These are idealized dipoles for computer simulations only and do not represent any cardiac activation. The choice of +1 and −1 V was used so that computed results can be easily scaled to other values.

The potential and current distributions in the whole torso were computed for two cases using the dipole as a boundary condition. In one case the anisotropic, and in the other case isotropic myocardial tissue resistivities were used. Isotropic tissue resistivities were used for all other tissue types and were kept the same in both cases. These resistivity values are available in the literature (Geddes and Baker 1967, Foster and Schwan 1989), have been used by us previously (Ramon *et al* 1998, 2000) and are summarized in table 1. Body surface potentials were extracted from the computed whole torso potentials. These were then used for contour plots of anterior and posterior BSPMs.

Statistical analyses of the data were performed to test whether the differences found in the simulated BSPMs obtained with anisotropic and isotropic myocardial conductivities were significant. The Kolmogorov–Smirnov (K–S) test was performed on the empirical distribution functions of the BSPM values. This K–S test examines the difference in the probability distribution of two independent samples (Press *et al* 1992). The BSPM data were arranged in continuously increasing order and their probability distributions, i.e. empirical distribution functions, were computed. The null hypothesis that the probability distributions of the two data sets are identical within a 5% limit was rejected when the p-value was less than 0.05. In other words, for $p < 0.05$ the K–S test showed that the BSPMs for anisotropic and isotropic cases were different. For $p > 0.05$, the BSPMs for the two cases were considered to be similar. Histogram and cumulative histogram analyses of the data

Table 1. Conductivity/resistivity values of the major tissue types used in the computer model of heart and torso.

Tissue type	Conductivity (mS cm^{-1})	Resistivity (Ω cm)
Lungs	0.667	1 500
Muscle	1.43	700
Fat	0.4	2 500
Connective tissue	2.22	450
Liver	1.2	834
Stomach	1.25	800
Blood	6.49	154
Hard bone	0.0625	16 000
Soft bone	0.459	2 178
Isotropic myocardium	2.38	420
Anisotropic myocardium		
Along fibre direction	7.604	131.5
Transverse to fibre direction	1.319	758
Atria	2.381	420
Spleen	0.1	10 000
Kidney	1.49	671
Gut	1.25	800
Skin	0.667	1 500
Soft tissues, diaphragm, nerve (spinal cord)	1.736	576
Oesophagus	1.429	700
Intestinal fluid	100	10

were also performed. The histogram distribution was obtained by binning the data in ten equally spaced bins and the cumulative histogram is the plot of the empirical distribution function.

We computed the correlation coefficient (CC) and the relative root-mean-square error (RE) also for the anisotropic and isotropic body surface potentials. The CC is a measure of the linear fit between two data sets and the RE is computed as

$$\mathrm{RE} = \sqrt{\frac{\sum (V_{\mathrm{aniso}} - V_{\mathrm{iso}})^2}{\sum (V_{\mathrm{aniso}})^2}} \tag{1}$$

where V_{aniso} are anisotropic and V_{iso} are isotropic body surface potentials, and the summation is over all sampling points located on the body surface. Here anisotropic BSPMs refer to the BSPM values computed with anisotropic myocardial conductivities. Similarly, isotropic BSPMs refer to the BSPM values computed with isotropic myocardial conductivities. A total of 21 134 body surface points were used for analysis. A value of RE near zero will indicate that the anisotropic and isotropic body surface potentials are similar, while a nonzero value will indicate otherwise.

All computations were performed on an Intel Pentium III, 350 MHz, two CPUs and a 512 MB memory workstation running a Linux operating system. An average run took about 30 min for computing the potential and current distribution in the whole torso. The post-processing and visualization of the data were done with Matlab 6.1 software (Mathworks, Inc., Natick, MA).

Table 2. Minimum, maximum, mean and STDs of the anisotropic and isotropic body surface potentials for dipoles in the heart wall. All minimum, maximum and mean STD values are in millivolts (mV). The last two columns list the CC and RE.

Dipole position	Anisotropic BSPMs (mV)			Isotropic BSPMs (mV)				
	Min	Max	Mean ± STD	Min	Max	Mean ± STD	CC	RE
LV wall								
x dipole	−0.48	1.0	−0.09 ± 0.3	−0.29	0.611	0.0 ± 0.17	0.965	1.13
y dipole	−0.53	0.06	−0.07 ± 0.1	−0.55	0.08	−0.05 ± 0.12	0.963	0.237
z dipole	−0.24	0.42	0.11 ± 0.14	−0.12	0.31	0.08 ± 0.09	0.944	0.23
RV wall								
x dipole	−0.34	0.22	0.03 ± 0.12	−0.32	0.17	0.0 ± 0.1	0.948	1.02
y dipole	−0.66	0.05	−0.46 ± 0.11	−0.36	0.03	−0.03 ± 0.06	0.992	0.317
z dipole	−0.25	0.45	0.07 ± 0.12	−0.09	0.24	0.03 ± 0.05	0.967	0.47
Septum								
x dipole	−0.8	0.47	0.0 ± 0.24	−0.52	0.35	0.0 ± 0.17	0.996	0.57
y dipole	−0.7	0.1	−0.04 ± 0.14	−0.57	0.07	−0.05 ± 0.11	0.98	0.096
z dipole	−0.09	0.5	0.11 ± 0.12	−0.06	0.31	0.08 ± 0.08	0.97	0.304
Apex								
x dipole	−0.38	0.93	0.0 ± 0.23	−0.52	0.48	0.0 ± 0.16	0.809	0.454
y dipole	−1.47	0.1	−0.11 ± 0.23	−1.1	0.03	−0.07 ± 0.16	0.881	0.351
z dipole	−0.9	0.84	0.19 ± 0.33	−0.3	0.5	0.1 ± 0.13	0.972	0.498

3. Results

A summary of the results is given in table 2. It lists the minimum, maximum, mean ± standard deviation (STD) of the anisotropic and isotropic BSPMs, the correlation coefficient and RE of the anisotropic and isotropic BSPMs. Using K–S tests, we found that BSPMs for the anisotropic and isotropic cases were different ($p < 0.01$) for all dipole positions and orientations. The correlation coefficients are in the range of 0.944 to 0.992 for the dipoles in the septum, LV wall and RV wall. For dipoles in the apical area of the heart, the correlation coefficients are in the range of 0.809 to 0.972. This would suggest that the fibre anisotropy in the apical area of the heart strongly influences the BSPMs. More details for individual dipole cases are given below. The contour plots and histogram plots of the anterior and posterior BSPMs for a few representative examples are also described below.

3.1. LV wall dipoles

Anterior and posterior BSPMs for an *x*-oriented dipole in the LV wall are shown in figure 2 and its corresponding histogram analysis is summarized in figure 3. The top row of plots in figure 2 is for the case where myocardium is anisotropic, the middle row is for the case where myocardium is isotropic, and the bottom row is for the difference of the two. The maximum and minimum contour values in millivolts are also given in each plot. The maximum and minimum values for the anisotropic case are greater than those for the isotropic case. For the anterior plot, the zero-crossing line of the contours is almost vertical for the isotropic case, but slightly leaning towards the right from the vertical for the anisotropic case. The differences are more visible in the difference plots (bottom row) and are similar to the anisotropic case (top row). This suggests that myocardial anisotropy does influence the BSPMs for an *x*-oriented dipole in the LV wall.

A histogram plot of the BSPMs is shown in figure 3. The left plot is the histogram distribution and the right plot is the cumulative histogram distribution of BSPMs. Both

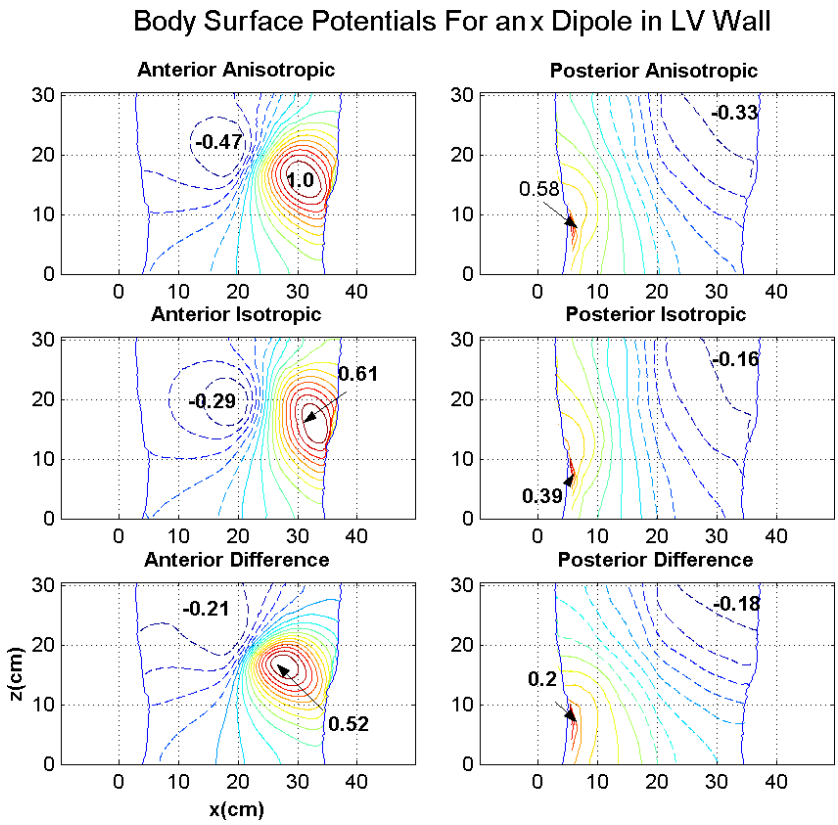

Figure 2. Contour plots of the BSPMs for an x-oriented dipole in the LV wall. Top row is for anisotropic anterior and posterior BSPMs, middle row is for isotropic anterior and posterior BSPMs and the bottom row is the difference of the anisotropic and isotropic cases. All values are in mV.

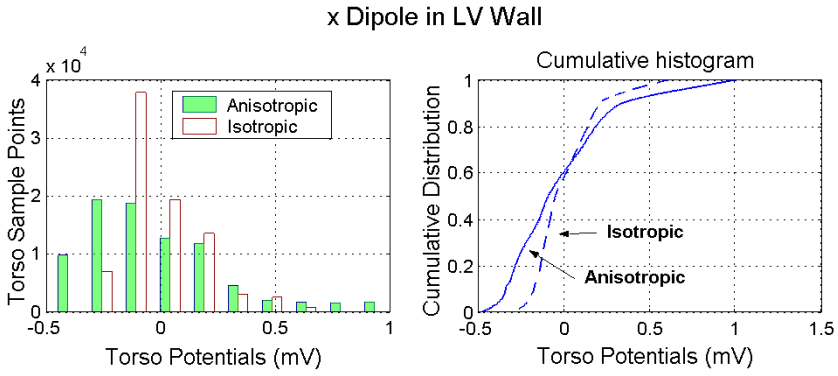

Figure 3. Histogram analysis of the body surface potentials for the x-oriented dipole in the LV wall. Left, histogram and right, cumulative histogram.

histogram plots show that the BSPMs are different for the anisotropic and isotropic cases. The majority of histogram distribution points for the anisotropic case are in the range of -0.5 to 0.2 mV with a peak around -0.2 mV while those for the anisotropic case are in the range of -0.1 to 0.2 mV with a peak around -0.1 mV. The cumulative histogram distribution also

shows a similar pattern; a steeper slope in the range of -0.5 to 0.2 mV and a less steep slope in the range of 0.2 to 1.0 mV. These differences in histogram distribution are also reflected in the mean $\pm$ STD values for this dipole given in table 2. The mean $\pm$ STD is -0.09 ± 0.3 mV for the anisotropic case and -0.0 ± 0.17 mV for the isotropic case. Because of the differences in the histogram distributions, the RE of 1.13 is also high for the *x*-oriented dipole in the LV wall.

Contour plots of the BSPMs for the *y*- and *z*-oriented dipoles in the LV wall are not shown. However, a summary of the results is given in table 2. The minimum and maximum values for the anisotropic and isotropic BSPMs for the *y*-oriented dipole in the LV wall are very similar. The correlation coefficient is 0.963 and the RE is 0.237. These values suggest that for a *y*-oriented dipole in the LV wall, myocardial anisotropy has some noticeable effect on BSPMs but not as strong as that for the *x*-oriented dipole in the LV wall.

For the *z*-oriented dipole, the minimum and maximum values for anisotropic BSPMs are -0.24 and 0.42, and for the isotropic BSPMs these are -0.12 and 0.31, respectively. The dynamic range between the maximum and minimum values is higher for the anisotropic BSPMs compared to that for the isotropic BSPMs. This is also reflected in the mean and STD values of the anisotropic (0.11 ± 0.14 mV) and isotropic (0.08 ± 0.09 mV) BSPMs. Both values are slightly higher for the anisotropic compared to the isotropic BSPMs. The correlation coefficient and the RE are 0.944 and 0.299, respectively. These values suggest that the BSPMs for a *z*-oriented dipole in the LV wall are affected by the myocardial anisotropy.

3.2. RV wall dipoles

The contour plots of the BSPMs for an *x*-oriented dipole in the RV wall are shown in figure 4 and their histogram distributions are given in figure 5. The anterior contour plots show a dipolar pattern with well defined positive and negative peaks which are not visible in the posterior contour plots. The positions of the peaks in the anterior contour plots show a very notable shift between the anisotropic and isotropic cases. The zero-crossing line is almost vertical for the isotropic case while for the anisotropic case it is slightly leaning towards the left from the vertical position. The differences between the anisotropic and isotropic cases are very well defined and recognizable in the difference plots (the bottom row of plots in figure 4). The histogram distribution (left-hand side in figure 5) is also different for the anisotropic and isotropic cases. The slopes of the cumulative histogram distributions for the anisotropic and isotropic cases are also different. The correlation coefficient and relative error are 0.948 and 1.02, respectively. These values suggest that the myocardial anisotropy does influence the BSPMs for an *x*-oriented dipole in the RV wall.

The contour plots and the histogram distributions of the BSPMs for the *y*- and *z*-oriented dipoles in the RV wall dipoles are not shown, but the summary of their results is given in table 2. The minimum, maximum and mean values of the anisotropic and isotropic BSPMs are different, suggesting that the myocardial anisotropy influences the BSPMs for the *y* and *z* dipoles located in the RV wall. The CC and RE for *x, y* and *z* dipoles in the RV wall are in the ranges 0.948–992 and 0.47–1.02, respectively. The *x*-oriented dipole has the lowest CC of 0.948 and the highest RE of 1.02. These values suggest that the myocardial anisotropy strongly influences the BSPMs for an *x*-oriented dipole in the RV wall. The CC of the BSPMs for the *y*-oriented dipole is 0.992, which would suggest that the myocardial anisotropy has very little effect on BSPMs for this particular dipolar source in the RV wall.

3.3. Dipoles in the septum

For an *x*-oriented dipole in the septum, the contour plots of the BSPMs are given in figure 6. The dipole orientation is from the subject's right to the left and due to this contour plots

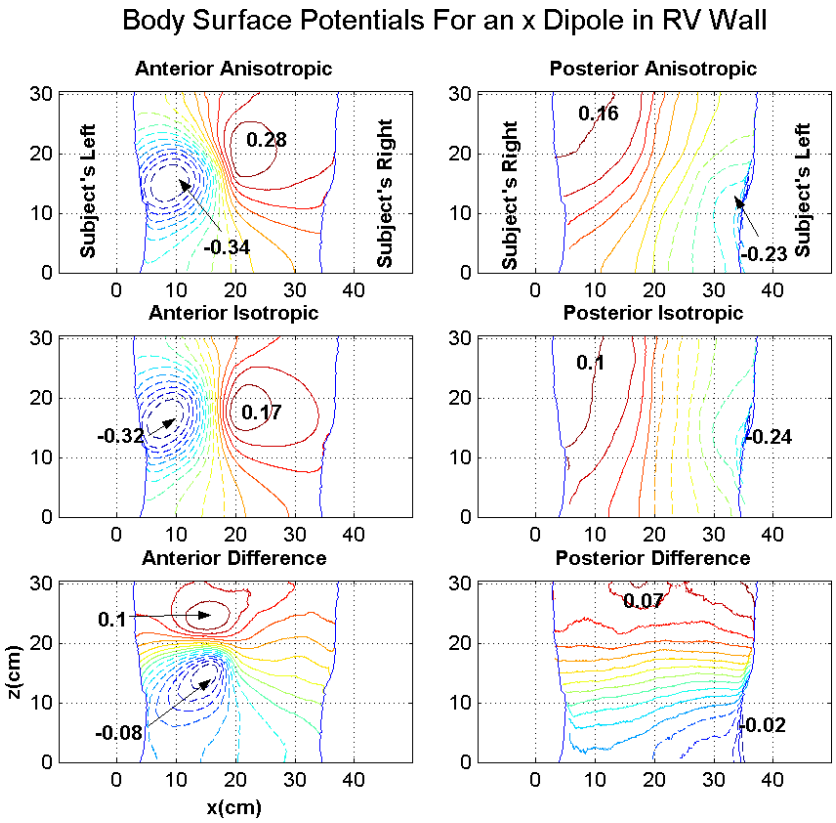

Figure 4. Contour plots of the BSPMs for an *x*-oriented dipole in the RV wall. Top row is for anisotropic anterior and posterior BSPMs, middle row is for isotropic anterior and posterior BSPMs and the bottom row is the difference of the anisotropic and isotropic cases. All values are in mV.

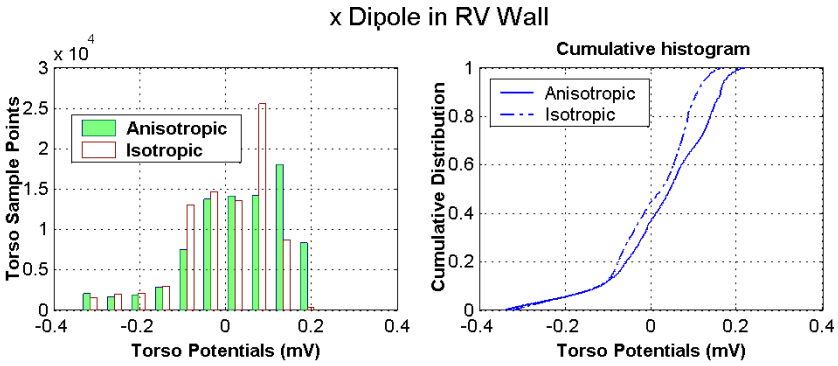

Figure 5. Histogram analysis of the body surface potentials for the *x*-oriented dipole in the RV wall. Left, histogram and right, cumulative histogram.

show very well-defined positive and negative peaks in the anterior torso plots. Since the heart is much closer to the front (anterior) of the torso, the contour peaks are well defined in the anterior plots compared to the posterior plots. The anisotropic contour peaks are more negative compared to the isotropic peaks in the plot. However, the shapes of the contours are very

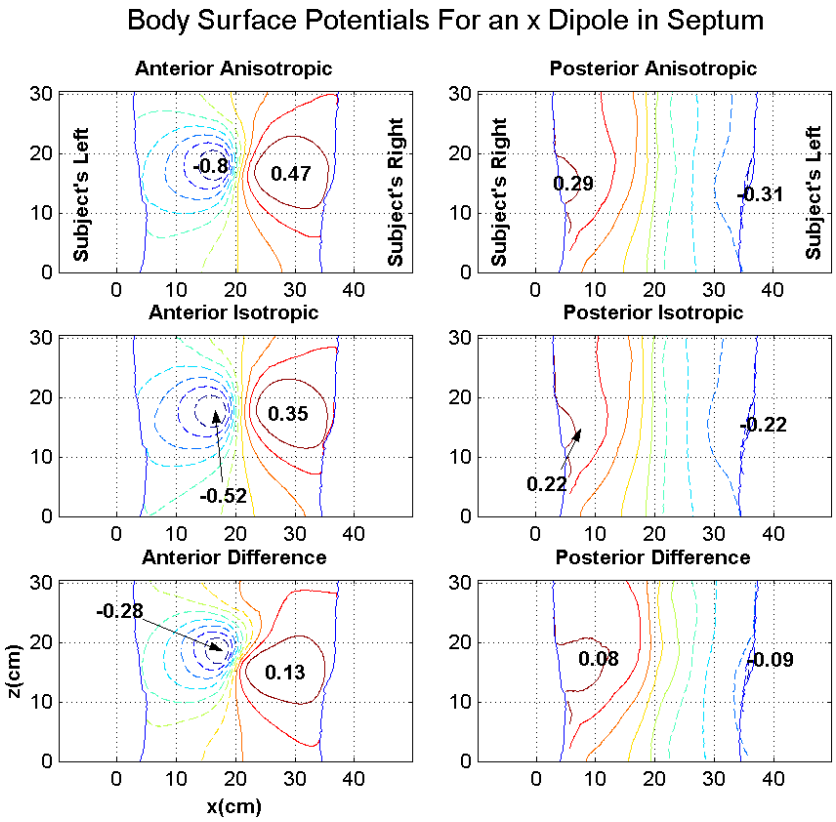

Figure 6. Contour plots of the BSPMs for an *x*-oriented dipole in the septum. Top row is for anisotropic anterior and posterior BSPMs, middle row is for isotropic anterior and posterior BSPMs and the bottom row is the difference of the anisotropic and isotropic cases. All values are in mV.

similar for the anisotropic and isotropic cases with the zero-crossing line almost vertical. The differences in the peak values and in the contour shapes are more visible in the bottom row of the plots. The histograms and the cumulative histogram distributions are shown in figure 7. The histogram distributions between the two cases are only slightly different which is also reflected in the high value of the correlation coefficient, 0.996.

For an *x*-oriented dipole in the septum, the minimum and maximum BSPM values are larger for the anisotropic case compared to the isotropic case. The same pattern is also present for the *y*- and *z*-oriented dipoles. The CC is 0.996 and RE is 0.57 for the *x*-oriented dipole in the septum. The RE value is high for the *x*-oriented dipole compared to the *y*- and *z*-oriented dipoles in the septum. The mean $\pm$ STD of the BSPMs for the anisotropic and isotropic cases are 0.0 ± 0.24 and 0.0 ± 0.17 respectively for the *x*-oriented dipole. The mean values are 0.0 for both cases, but the STD is different. This difference in STD also shows up as a larger RE value of 0.57 for the *x*-oriented dipole in the septum.

3.4. Dipoles in the apex

Figure 8 shows the contour plots of BSPMs for an *x*-oriented dipole in the apical area of the heart wall. Here the differences between the anisotropic and isotropic cases are very pronounced. The location of the peaks and their values are different for the anisotropic and

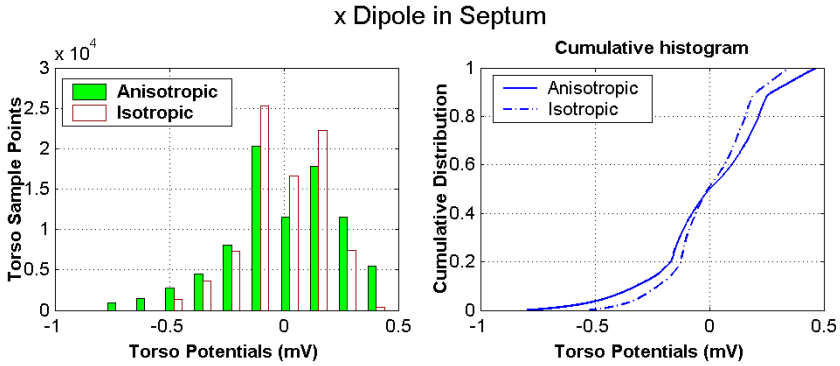

Figure 7. Histogram analysis of the body surface potentials for the *x*-oriented dipole in the septum. Left, histogram and right, cumulative histogram.

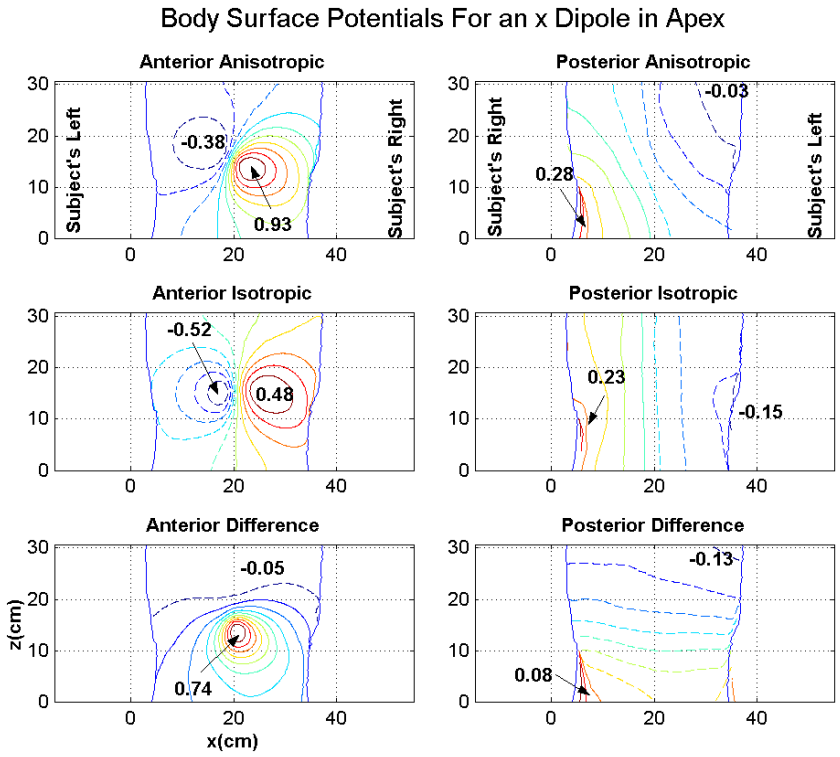

Figure 8. Contour plots of the BSPMs for an *x*-oriented dipole in the apical area of the heart wall. Top row is for anisotropic anterior and posterior BSPMs, middle row is for isotropic anterior and posterior BSPMs and the bottom row is the difference of the anisotropic and isotropic cases. All values are in mV.

isotropic cases. The zero-crossing line is almost vertical for the isotropic case while it is almost at 70° for the anisotropic case. The histogram distributions are given in figure 9. The correlation coefficient is 0.809 which is the lowest compared to all other dipole locations in the heart wall. The histogram distributions do show differences between the anisotropic and the isotropic case.

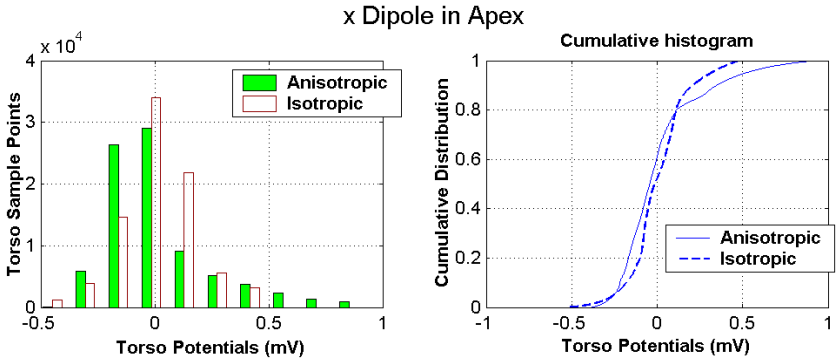

Figure 9. Histogram analysis of the body surface potentials for the *x*-oriented dipole in the apical area of the heart wall. Left, histogram and right, cumulative histogram.

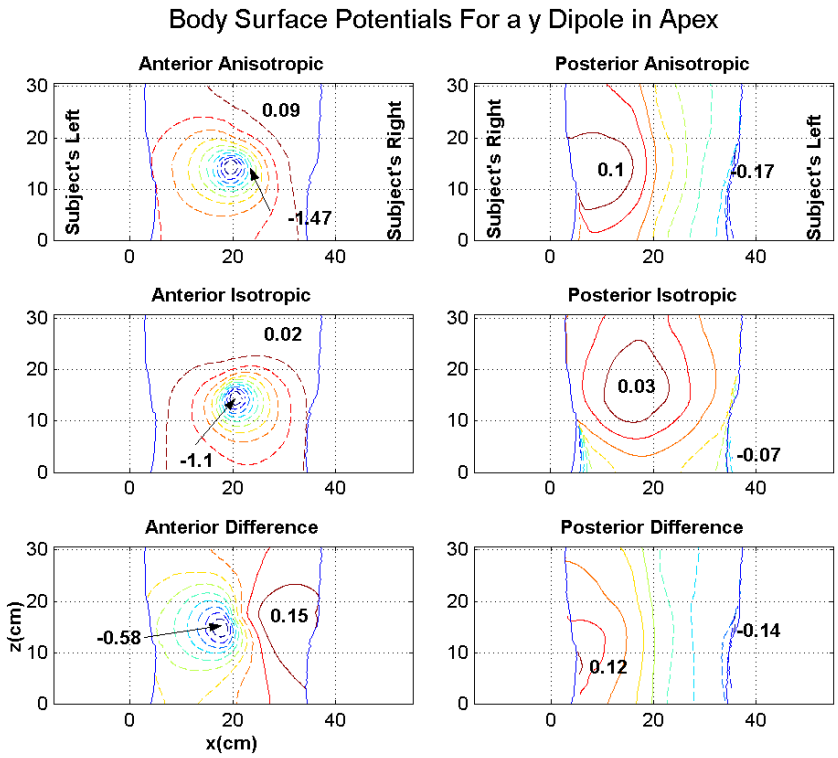

Figure 10. Contour plots of the BSPMs for a *y*-oriented dipole in the apical area of the heart wall. Top row is for anisotropic anterior and posterior BSPMs, middle row is for isotropic anterior and posterior BSPMs and the bottom row is the difference of the anisotropic and isotropic cases. All values are in mV.

For a *y*-oriented dipole, the contour plots are shown in figure 10. The negative peak values are lower for the anisotropic case compared to the isotropic case. The histogram distributions are given in figure 11 and these look very similar for the isotropic and anisotropic cases. The correlation coefficient is also low for this case with a value of 0.881. For a *z*-oriented dipole, the contour plots are shown in figure 12. Here the dipolar pattern of the contour plots is

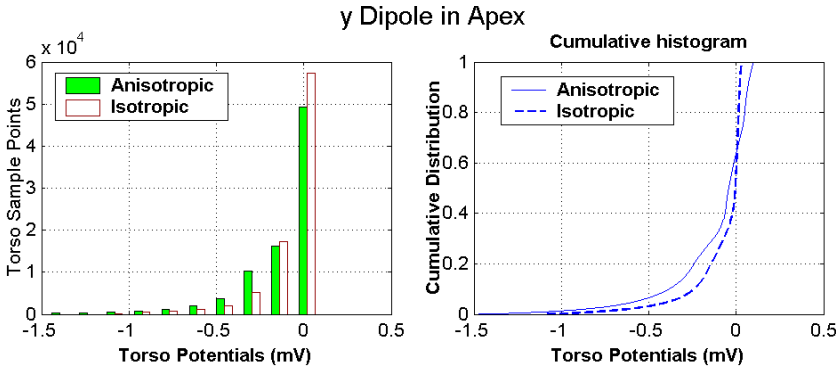

Figure 11. Histogram analysis of the body surface potentials for the y-oriented dipole in the apical area of the heart wall. Left, histogram and right, cumulative histogram.

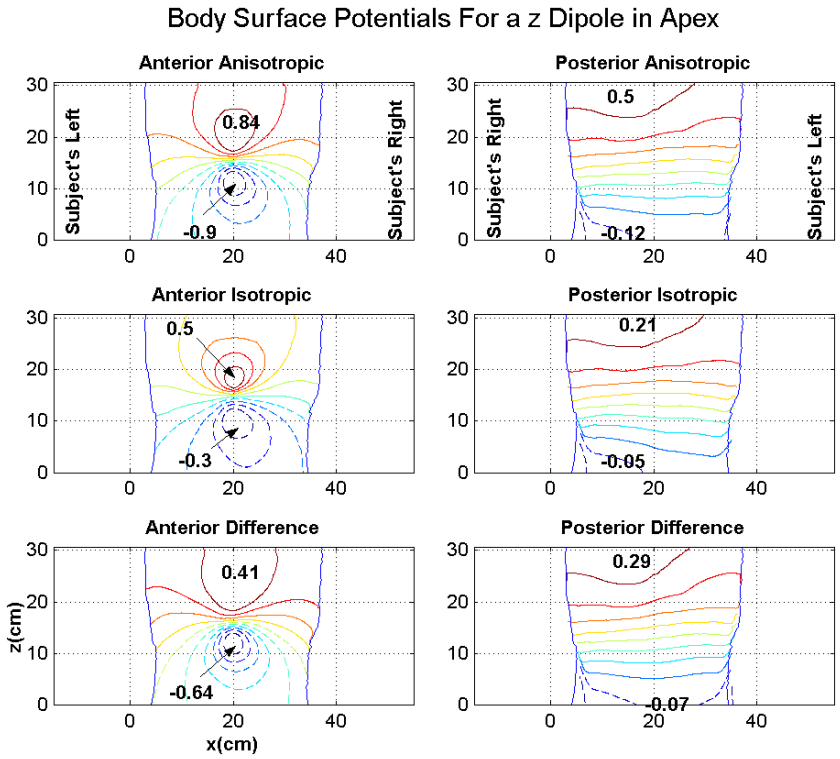

Figure 12. Contour plots of the BSPMs for a z-oriented dipole in the apical area of the heart wall. Top row is for anisotropic anterior and posterior BSPMs, middle row is for isotropic anterior and posterior BSPMs and the bottom row is the difference of the anisotropic and isotropic cases. All values are in mV.

very visible. Once again the anisotropic peak values are larger in magnitude compared to isotropic peak values. The locations of the peaks and the zero-crossing lines do not show a large difference between the anisotropic and isotropic cases. The differences in the histogram distribution are shown in figure 13. For this case the correlation coefficient is 0.972 and the RE is 0.498. A summary of the results is tabulated in table 2. The apical dipoles have very

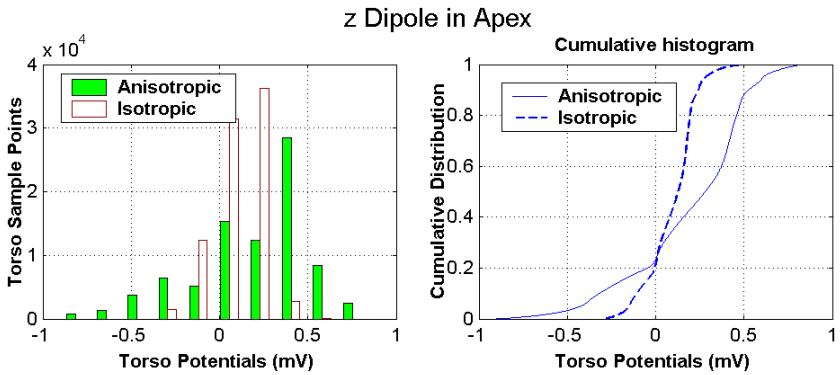

Figure 13. Histogram analysis of the body surface potentials for the z-oriented dipole in the apical area of the heart wall. Left, histogram and right, cumulative histogram.

low correlation coefficients, suggesting that myocardial fibre orientation strongly influences the BSPMs for the sources located in the apical area of the heart wall.

4. Discussion

We have examined the effect of myocardial anisotropy on the body surface potentials due to dipolar sources in different areas of the heart wall. This complements our previous study (Ramon *et al* 2000) in which we studied the effects of myocardial anisotropy only for a z-oriented dipole in the septum of the heart wall. In particular, the most significant contribution is the analysis of anisotropy effects on BSPMs due to the dipolar sources in the apical area of the heart where the myocardial fibre structure has a loop-like structure (Torrent-Guasp 1998, Streeter 1979). The results reported here show that myocardial anisotropy influences the BSPMs for the dipoles situated in different areas of the heart wall. Dynamic ranges of the BSPMs for the anisotropic case are higher than the ranges in the isotropic case. These results confirm earlier suggestions made in the literature that the orientation of myocardial fibres could influence the current flow patterns and the electrical potentials in the heart and torso (Plonsey 1974, Streeter 1979, Taccardi *et al* 1997, Colli-Franzone *et al* 1998, Hren *et al* 1998a). These findings suggest that the orientations of the cardiac muscle fibres should be included in the heart–torso models for an accurate modelling of the volume current and also for improved modelling of the BSPMs.

The anisotropy effects are strongest for the dipoles in the apical area of the heart. This could be due to the fact that, in the apical area of the heart, fibre orientation goes almost through a 300° rotational change. Following the anatomical fibre patterns, one could say that fibres coming from one side of the heart, say the LV wall, traverse almost a double-helix loop-like pattern in the apical area of the wall and then continue onwards to the RV wall of the heart (Torrent-Guasp 1998, Streeter 1979, Schmid *et al* 1997). Such a change in the structural pattern of the myocardial fibres will certainly influence the current flow patterns and, subsequently, the potentials on the torso surface.

We have used a highly heterogeneous model of the heart and torso that includes the major tissue types in the torso, a detailed structure of the heart chambers and the myocardial fibre orientations. Such a highly heterogeneous high-resolution model provides a detailed account of the volume current flow patterns in the torso and is necessary for examining

the effect of myocardial fibres on the BSPMs. In a recent study it has been shown that relative to a homogeneous torso, an inhomogeneous torso model has some minor effects on BSPM patterns (Ramanathan and Rudy 2001). These minor effects on BSPMs could be modified (or amplified) if one uses myocardial anisotropy in the model which will modify the spreading of the volume currents within the myocardium and emanating out of the epicardium. This myocardial anisotropy related spread of the currents was documented earlier by us (Ramon *et al* 2000) and, probably, could be one of the possible causes of the observed changes in the BSPMs. A major shortcoming of our model is that we have used only idealized +1 and −1 V dipolar sources. Moreover, we have used only one source active at a time. The effects of myocardial anisotropy on ECG/MCG modelling should also be examined in detail by using multiple sources in the heart wall.

An earlier study has been reported in the literature with mixed results. Wei *et al* (1995a, 1995b) have examined the effect of anisotropy on the heart excitation and on the body surface electrocardiograms. Their figures do show some anisotropy-dependent changes even though they did not mention this in their paper. One reason could be that they were looking for gross polarity changes in simulated body surface electrocardiograms. Other reasons that they did not observe significant changes could be related to the larger smoothing effects of a simplified model of the torso compared to a highly heterogeneous model of the torso, and that they used only a limited range of 0°–90° of myocardial fibre orientations in the heart wall. In general, myocardial orientation changes almost by 180° in traversing from epicardium to endocardium (Streeter 1979, Schmid *et al* 1997).

Other related studies have examined the effect of myocardial tissue anisotropy on the epicardial potentials (Hren *et al* 1998a) and also on the wavefront propagation in the heart wall (Thivierge *et al* 1997). Thivierge *et al* (1997) studied the effect of myocardial anisotropy with an equivalent heart dipole. Their hypothesis was that inclusion of anisotropy adds an axial dipole component oriented along the fibres. They found that the effects related to the myocardial anisotropies were diminished when the myocardial tissue conductivities were close to the torso conductivities. Our modelling parameters are a bit different and so we are unable to compare our results with those of Thivierge *et al* (1997). However, myocardial anisotropy and torso inhomogeneity related changes would certainly be diminished if one uses the myocardial tissue conductivity similar in value to that of torso conductivity.

Using a spherical model of the heart and torso, it was shown by Schmidt and Pilkington (1991) that the myocardial anisotropy has a significant effect on the magnitude of the body surface potentials. Also, in a recent review (Taccardi *et al* 1997) it was suggested that myocardial fibre structure plays an important role in the electrical activity of the myocardium. In addition, there are computer models of the heart available (Huiskamp 1998, Lorange and Gularjani 1993, Siregar *et al* 1998) that include myocardial tissue anisotropy. These computer models have been used for simulation of the epicardial potentials and electrocardiograms but have not been used to quantify, in detail, the effects of myocardial anisotropy on body surface potentials.

We have used a highly heterogeneous model of the heart and torso to model the effect of volume currents. This is a good model to quantify changes in BSPMs due to volume currents, but still far away from the realities of a subject-specific model of a person. In real life situations, the conductivity values could be very different from those used here and the myocardial fibre structure could also be different. The effect of tissue conductivity changes on the torso magnetic fields has been examined previously by us (Czapski *et al* 1996a) using a heart–torso model similar to what we have used here. Our earlier results (Czapski *et al* 1996b) show that the torso magnetic fields are very sensitive to changes in the conductivity of blood and myocardium, and less sensitive to the conductivity of the lungs, muscle, fat and other

tissues. One could expect similar conductivity related changes in BSPMs. The myocardial fibre orientations could also differ from one subject to another and should be incorporated in a subject-specific fashion. Such information can be obtained from the diffusion tensor magnetic resonance imaging of the heart (Reese *et al* 1995, Tseng *et al* 2000). Thus, the results reported here provide a general pattern of how myocardial anisotropy affects the BSPMs. For a particular subject, one needs to modify our results by using subject-specific tissue conductivities and the myocardial fibre structure. Subject-specific tissue conductivities for the myocardium can be obtained from the diffusion tensor MRI data but for the other tissues one has to rely on the older published values (Geddes and Baker 1967, Foster and Schwan 1989).

Body surface potentials show some changes related to the body habitus (Green *et al* 1985), with the position of the heart in the body (MacLeod *et al* 2000), and also with the displacements of BSPM leads (Jazbinsek and Hren 1999). These changes related to body habitus or displacement of the leads could overshadow the anisotropy related changes in the BSPMs. This will be less of a problem in computer simulation experiments where one knows the anatomical shape of the torso, location of the heart and the location of the leads on the body surface. However, in experimental verification of anisotropy related effects on BSPMs, one needs to account for these effects.

In summary, our results show that the body surface potentials are influenced by the myocardial fibre anisotropy and, perhaps, one should include myocardial anisotropy when modelling the electrical activity of the human heart. In principle, the inclusion of fibre orientation might also be necessary for solving the cardiac inverse problem for localizing the sources of electrical activity in the heart. However, this needs to be investigated.

Acknowledgments

This work was supported in part by the National Science Foundation grants INT-9726712 and 0112742, the NIH grant R55-RR13301 and an equipment grant from the Seattle Foundation.

References

Aiba T, Inagaki M, Shimizu W, Matsuo K, Taguchi A, Suyama K, Kurita T, Aihara N, Sunagawa K and Kamakura S 2000 Recovery time dispersion measured from 87-lead body surface potential mapping as a predictor of sustained ventricular tachycardia in patients with idiopathic dilated cardiomyopathy *J. Cardiovasc. Electrophysiol.* **11** 968–74

Colli-Franzone P, Guerri L, Pennacchio M and Taccardi B 1998 Spread of excitation in 3-D models of the anisotropic cardiac tissue: III. Effects of ventricular geometry and fiber structure on the potential distribution *Math. Biosci.* **151** 51–98

Czapski P, Ramon C, Haueisen J, Huntsman L L, Nowak H, Bardy G H, Leder U and Kim Y 1998 MCG simulations of myocardial infarctions with a realistic heart–torso model *IEEE Trans. Biomed. Eng.* **45** 1313–21

Czapski P, Ramon C, Huntsman L L, Bardy G H and Kim Y 1996a Effects of tissue conductivity variations on the cardiac magnetic fields simulated with a realistic heart–torso model *Phys. Med. Biol.* **41** 1247–63

Czapski P, Ramon C, Huntsman L L, Bardy G H and Kim Y 1996b On the contribution of volume currents to the total magnetic field resulting from the heart excitation process: a simulation study *IEEE Trans. Biomed. Eng.* **44** 95–104

Eason J, Schmidt J, Dabasinskas A, Siekas G, Aguel F and Trayanova N 1998 Influence of anisotropy on local and global measures of potential gradient in computer models of defibrillation *Ann. Biomed. Eng.* **26** 840–9

Foley T A 1995 Deformation of volumes using scattered landmark points *Intelligent Systems: Third Golden Int. Conf.—Edited and Selected Papers* ed E A Yfantis (Norwell: Kluwer) pp 841–51

Foster K R and Schwan H P 1989 Dielectric properties of tissues and biological materials: a critical review *CRC Crit. Rev. Biomed. Eng.* **17** 25–104

Geddes L A and Baker L E 1967 The specific resistance of biological material *Med. Biol. Eng.* **5** 271–93

Green L S, Lux R L, Haws C W, Williams R R, Hunt S C and Burgess M J 1985 Effects of age, sex, and body habitus on QRS and ST-T potential maps of 1100 normal subjects *Circulation* **71** 244–53

Green L S, Lux R L, Haws C W, Williams R R, Hunt S C and Burgess M J 1986 *Circulation* **74** 785 (erratum)

Hren R, Nenonen J and Horacek B M 1998a Simulated epicardial potential maps during paced activation reflect myocardial fibrous structure *Ann. Biomed. Eng.* **26** 1022–35

Huiskamp G 1998 Simulation of depolarization in a membrane-equation based model of the anisotropic ventricle *IEEE Trans. Biomed. Eng.* **45** 847–55

Hren R, Stroink G and Horacek B M 1998b Accuracy of single-dipole inverse solution when localising ventricular pre-excitation sites: simulation study *Med. Biol. Eng. Comput.* **36** 323–9

Hren R, Zhang X and Stroink G 1996 Comparison between electrocardiographic and magnetocardiographic inverse solutions using the boundary element method *Med. Biol. Eng. Comput.* **34** 110–14

Jazbinsek V and Hren R 1999 Influence of randomly displaced BSPM leads on the identification of ventricular pre-excitation sites *Biomed. Tech.* **44** (Suppl. 2) 104–7

Lorange M and Gularjani R M 1993 A computer heart model incorporating anisotropic propagation: I. Model construction and simulation of normal activation *J. Electrocardiol.* **26** 245–61

MacLeod R S, Ni Q, Punske B, Ershler P R, Yilmaz B and Taccardi B 2000 Effects of heart position on the body-surface electrocardiogram *J. Electrocardiol.* **33** (Suppl.) 229–37

Nielsen P M F, Le Grice I J, Smaill B H and Hunter P J 1991 Mathematical model of geometry and fibrous structure of the heart *Am. J. Physiol.* **260** H1365–78

Pinter A, Molin F, Savard P, Tremblay G, Sierra G and Nadeau R 2000 Body surface mapping of retrograde P waves in the intact dog by simulation of accessory pathway re-entry *Can. J. Cardiol.* **16** 175–82

Plonsey R 1974 An evaluation of several cardiac activation models *J. Electrocardiol.* **7** 237–44

Press W T, Teukolsky S A, Vetterling W T and Flannery B P 1992 *Numerical Recipes in C* (New York: Cambridge University Press) pp 623–8

Ramanathan C and Rudy Y 2001 Electrocardiographic imaging: I. Effect of torso inhomogeneities on body surface electrocardiographic potentials *J. Cardiovasc. Electrophysiol.* **12** 229–40

Ramon C, Czapski P, Haueisen J, Huntsman L L, Nowak H, Bardy G H, Leder U, Kim Y and Nelson J A 1998 MCG simulations with a realistic heart–torso model *IEEE Trans. Biomed. Eng.* **45** 1322–41

Ramon C, Wang Y, Haueisen J, Schimpf P, Ishimaru A and Jaruvatanadilok S 2000 Effect of myocardial anisotropy on torso current flow patterns, potentials and magnetic fields *Phys. Med. Biol.* **45** 1141–50

Reese T G, Weisskoff R M, Smith R N, Rosen B R, Dinsmore R E and Wedeen V J 1995 Imaging myocardial fiber architecture *in vivo* with magnetic resonance *Magn. Reson. Med.* **34** 786–91

Rush S, Abildskov J A and McFee R 1962 Resistivity of body tissues at low frequencies *Circ. Res.* **12** 40–50

Schimpf P, Haueisen J, Ramon C and Nowak H 1998 Realistic computer models of electric and magnetic fields of human head and torso *Parallel Comput.* **24** 1433–60

Schimpf P H, Haynor D R and Kim Y 1996 Object-free adaptive meshing in highly heterogeneous 3-D domains *Int. J. Biomed. Comput.* **40** 209–25

Schmid P, Niederer P, Lunkenheimer P P and Torrent-Guasp F 1997 The anisotropic structure of the left and right ventricles *Technol. Health Care* **5** 29–43

Schmidt J A and Pilkington T C 1991 The volume conductor effects of anisotropic muscle on body surface potentials using an eccentric spheres model *IEEE Trans. Biomed. Eng.* **38** 300–03

Shrinidhi N, Haynor D R, Wang Y, Jorgenson D B, Bardy G H and Kim Y 1996 An efficient tissue classifier for building patient-specific finite element models from x-ray CT images *IEEE Trans. Biomed. Eng.* **43** 333–7

Siregar P, Sineteff J P, Julen N and Le Beux P 1998 An interactive 3D anisotropic cellular automata model of the heart *Comput. Biomed. Res.* **31** 323–47

Streeter D D Jr 1979 Gross morphology and fiber geometry of the heart *Handbook of Physiology: A Critical, Comprehensive Presentation of Physiological Knowledge and Concepts* vol 1 ed R M Berne (Bethesda, MD: American Physiological Society) pp 61–112

Stroink G, Meeder R J, Elliott P, Lant J and Gardner M J 1999 Arrhythmia vulnerability assessment using magnetic field maps and body surface potential maps *Pacing Clin. Electrophysiol.* **22** 1718–28

Taccardi B, Lux R L, Ershler P R, Macleod R, Dustman T J and Ingebrigtsen N 1997 Anatomical architecture and electrical activity of the heart *Acta Cardiol.* **52** 91–105

Thivierge M, Gulrajani R M and Savard P 1997 Effects of rotational myocardial anisotropy in forward potential computations with equivalent heart dipole *Ann. Biomed. Eng.* **25** 477–98

Torrent-Guasp F 1998 Structure and function of the heart *Rev. Esp. Cardiol.* **51** 91–102

Tseng W Y, Reese T G, Weisskoff R M, Brady T J and Wedeen V J 2000 Myocardial fiber shortening in humans: initial results of MR imaging *Radiology* **216** 128–39

Wang Y, Haynor D R and Kim Y 2001 An investigation of the importance of myocardial anisotropy in finite element modeling of the heart: methodology and application to the estimation of defibrillation efficacy *IEEE Trans. Biomed. Eng.* **48** 1377–89

Wei D, Okazaki O and Harumi K 1995a Comparison of body surface potential maps simulated with isotropic and anisotropic computer heart models *J. Electrocardiol.* **28** 346–7

Wei D, Okazaki O, Harumi K, Harasawa E and Hosaka H 1995b Comparative simulation of excitation and body surface electrocardiogram with isotropic and anisotropic computer heart models *IEEE Trans. Biomed. Eng.* **42** 343–57